Long range boundary effect of 2D intermediate number density vibro-fluidized granular media in micro-gravity

2011 J. Phys.: Conf. Ser. 327 012033

(http://iopscience.iop.org/1742-6596/327/1/012033)

Journal of Physics: Conference Series **327** (2011) 012033 doi:10.1088/1742-6596/327/1/012033

Long range boundary effect of 2D intermediate number density vibro-fluidized granular media in micro-gravity

Chen Yanpei[1,2], Pierre Evesque[1], Meiying Hou[2], C. Lecoutre[3], F. Palencia[3] and Yves Garrabos[3]

[1] Lab MSSMat, Ecole Centrale de Paris,UMR 8579 CNRS, 92295 Châtenay-Malabry Cedex, France

[2] Institute of Physics, Chinese Academy of Sciences, Beijing, 100190, China

[3] ESEME, Institut de Chimie de la Matière Condensée de Bordeauz, CNRS UPR 9048, 33608 Pressac Cedex, France

E-mail: pierre.evesque@ecp.fr mayhou@aphy.iphy.ac.cn

Abstract. We present a micro-gravity experimental study of the statistical properties of intermediate number density vibro-fluidized inelastic spheres in a rectangular container. It is found that although when taking all the particles into account, the probability distributions of velocities both along and perpendicular to the vibration direction are exponential and symmetric, when dividing particles along the vibration direction into different bins, the local velocity distributions are found to deviate measurably from a symmetric distribution for the velocity component in the vibrating direction. The skewness analysis of the local distribution profiles for v_x and v_y shows that the local distribution of v_x remains symmetric, however, the skewness of the distribution profile in v_y changes nearly linear from positive to negative with skew = 0 near the center bin. This indicates a long range boundary effect of the asymmetry in v_y. We further studied the hydrodynamic profiles granular pressure p_x and p_y, and temperature T_x and T_y in positive and negative components such as p_x^+ and p_x^-, and T_x^+ and T_x^-, in accordance with the sign of velocity components. The profiles for the two components are found different along the y direction. Along vibration direction granular medium is found inhomogeneous and anisotropic not only in the particle number densities, but also in v_y, p_y and T_y. This suggests new hydrodynamical modeling is needed for such vibro-fluidized granular systems.

1. Introduction

Granular medium has caught much of physicists' attention in theoretical, simulation and experimental studies in recent years. It is deemed as an ideal model system for studying the statistical and dynamical properties of nonlinear non-equilibrium systems. Granular systems are treated by resembling the molecular gas or ordinary fluids [1] in many works although big differences may be found between them. For a nearly homogeneous granular system, it is assumed that the granular systems follow the Maxwell-Boltzmann velocity distribution $e^{-mv^2/2kT}$ and conform to equipartition of energy. From the Maxwell-Boltzmann distribution, temperature is defined by $T = 1/2m < v^2 > (k = 1)$, when there are no macroscopic flows in the system. However, an increasing number of works point out the non-Gaussian velocity distribution [2–11] in granular gases. These deviations from the Maxwell distribution find

overpopulation in the high-velocity tail. Kinetic reasons of these deviations are still unclear. Among all the potential reasons, concerns on the driving mechanism [6, 12–22] have been raised. Brey [21] discussed discontinuity effects at the sawtooth boundary in direct Monte Carlo simulation being due to the particle-number conservation near the boundary. Local distribution functions f at the boundary walls are found asymmetric and discontinuous. Olaf Herbst [22] et al. also found same local velocity distributions f in simulation. However, they did not indicate whether this asymmetry and discontinuity due to the boundary effect only existed in the 'Boundary Layer' or extended to the whole cell. If it extends to the whole cell, another question to ask is how it shall vary with the distance from the boundary. For inhomogeneous granular media whether hydrodynamic descriptions hold is unclear. Breakdowns of the hydrodynamics have been shown [23, 24]. To find the suitable scope of hydrodynamics for granular systems is still a challenge and further studies, especially experimental studies, are needed.

This paper reports our experimental observations obtained in Airbus of *Novespace* (2006 Campaign) in a 2D vibro-fluidized granular system. In the experiment the particle velocity distributions are obtained in both x and y directions globally and locally. It is found that although when taking all the particles into account, the probability distributions of velocities both along and perpendicular to the vibration direction are exponential and symmetric, but when dividing particles along the vibration direction into bins, the local velocity distribution measured in each bin is found to deviate measurably from a symmetric distribution for the velocity component in the vibrating direction. Considering the asymmetric distributions of local velocities, we measure hydrodynamic profiles in positive and negative components in accordance with the sign of velocity components. We find that the hydrodynamic profiles are different for these two components. Under the influence of the vibrating walls, granular medium is found inhomogeneous and anisotropic not only in the particle number density, but also in v_y, p_y and T_y.

The outline of this paper is as follows. In Section 2, we present the experimental method. In section 3, we show the global velocity distributions are exponential and symmetric in both x and y directions, but the local velocity distributions are asymmetric in the y direction and the skewness is discussed. In section 4, the distributions of hydrodynamic parameters are investigated. Finally, a brief summary is given.

2. Experimental Method

The experiment was conducted in Airbus A300 developed by *Novespace* in 2006. A quasi-2D quadrate cell (side walls in aluminum, front and back walls in glass, V=10mm *10mm *1.4 mm) containing 47 copper spheres is driven in y direction with a sinusoidal oscillating shaker. A snapshot is shown in Fig. 1. The diameter of the copper spheres is (1.21mm $\pm$ 0.02mm) , and the area fraction is 0.54. The spheres can rotate in three dimensions but only have two dimension translational motion.

The cell is fixed on a V455 LDS shaker, which vibrates in the y direction. The vibration controller is the same as in previous works [8,25]. The movement of the beads is recorded by a fast camera (499 fps). The LEDs are mounted in the reverse side of the cell to increase the contrast of the beads vs. the background. The experiments were performed for 30 parabolic flights in a 2-hour Campaign. Each parabolic flight has about 20s for micro-gravity (0.0 g$\pm$ 0.05 g). Within the 20s of each parabolic flight only one second is recorded by the fast camera. The resolution of the cell image is 288 pixel* 288 pixel, i.e. 1 pixel= 0.035mm. The frequency range in the experiment is from 40 Hz to 130Hz, the oscillating amplitude is ranged from 0.005 to 0.912mm, and the correspondent acceleration is in the range of 0.1 g to 9 g. In this paper, we only present four sets of data with vibrating conditions shown in Table 1. We use notations (A, V_ω, Γ, f) to represent amplitude, vibrating peak velocity, acceleration and frequency, respectively.

In the table all the parameters are determined by image analysis using the software *ImageJ*.

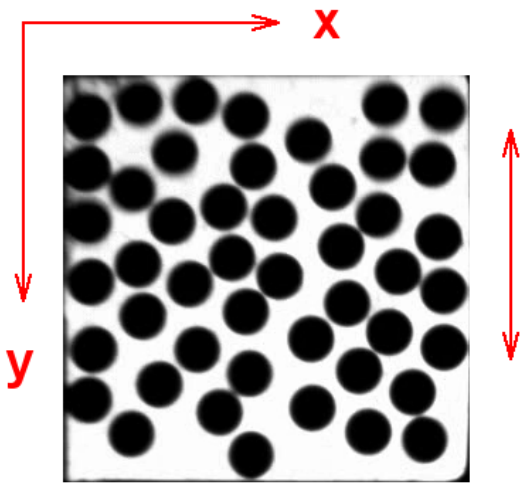

Figure 1: Snapshot of the cell particles. The cell contains 47 bronze sphere particles, driven in y direction at various vibration parameter(A, V_ω, Γ, f). The diameter of particle is 1.21 mm and cell size is (10mm*10mm*1.4mm).

Images recorded by the fast camera are firstly processed to get the positions of beads center which are calculated through the ultimate eroded points(UEPs) in the Euclidian distance map(EDM). Afterwards, particles are tracked using the program of minimum-distance algorithm. Since our system has moderate number density, the spheres can not move extensively, the minimum-distance algorithm can work well in our case. The magnitude of accuracy obtained in this way reaches $0.01mm$.

Table 1: The driving parameters in experimental. The y is the vibration direction (Amplitude A, speed $V_w = A\omega$, $\Gamma = A\omega^2$ for acceleration, frequency f).

	$Frequency(Hz)$	$A(0-peak,\ \ mm)$	$\Gamma(m/s^2)$	$V_\omega(m/s)$
1.	49	0.23	21.56	0.070
2.	97	0.11	41.28	0.067
3.	97	0.14	53.60	0.088
4.	49	0.12	11.73	0.038

3. Velocity distributions

In this section, the velocity distributions are analyzed under vibration condition 1 listed in ***Table 1***. The particle velocities are averaged for 499 image sequences within 1 second. Considering the anisotropy of the vibration, we analyze the x and y components of the velocity distributions separately. For local velocity distribution along vibrating axis, y axis, we divide the cell into seven bins and measure the velocity distribution in each bin.

3.1. The velocity distributions

The velocity distributions for components v_x and v_y are investigated as shown in Fig. 2. The velocities v_x and v_y are scaled by the characteristic velocities $v_c^x = \sqrt{\bar{v_x^2}} = \sqrt{T_x}$ and $v_c^y = \sqrt{\bar{v_y^2}} = \sqrt{T_y}$ [7], respectively. The velocity distributions in logarithmic scale are also shown in the insets of Fig. 2 (a) and (b). In the figures, the dash lines are exponential fitting $C * exp(-|B * x|)$, where A and B are fitting parameters, while the solid lines are Gaussian fitting $F * exp(-(x/G)^2)$, and F and G are fitting parameters. As can be seen in the figures, the Gaussian fitting underestimates in the parts of low and high velocities, in agreement with previous report [7]. The characteristic velocity $v_c^y = 0.057m/s$ is found larger than v_c^x $(0.041m/s)$. Anisotropy is apparent.

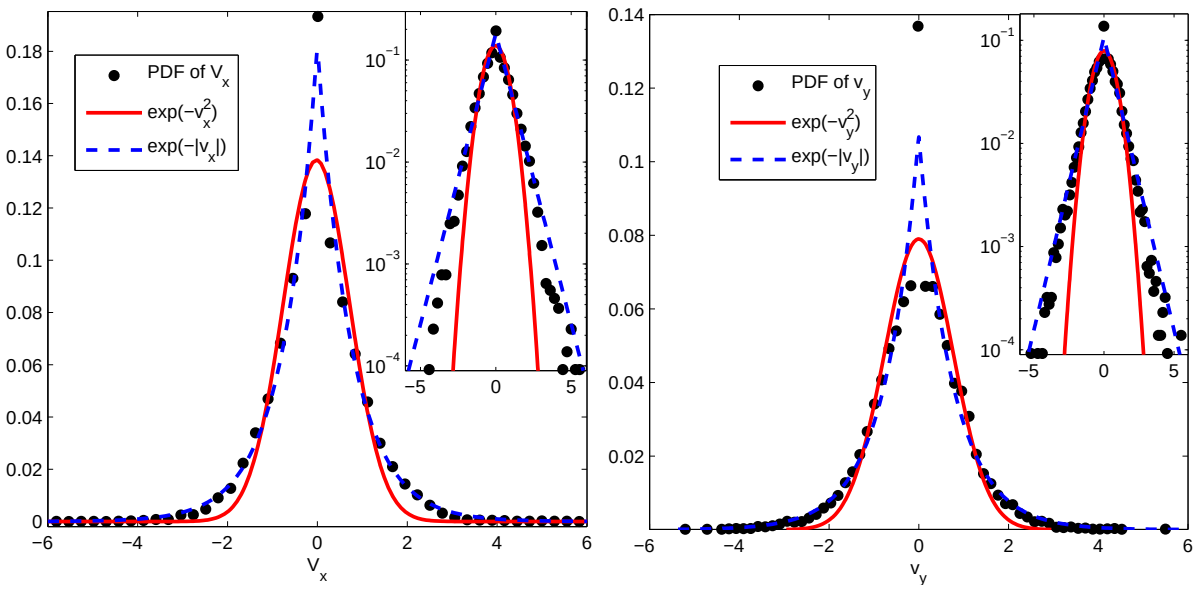

Figure 2: Distribution of the v_x (a) and v_y (b) in the experiment no. 1 of *Table 1*. The insets are the same plots on logarithmic scale. The velocities are scaled by $\sqrt{T_x} = 0.041m/s$ and $\sqrt{T_y} = 0.057m/s$. The solid lines are the Gaussian fit, where dashed lines are exponential.

3.2. Local velocity distributions

In order to understand the spatial distribution of velocities, the local velocity distributions are investigated. The cell is divided into 7 bins along the y axis, and the velocity distributions v_x and v_y are averaged in each bin. The velocity is scaled by the maximum driving velocity $V_\omega(0.07m/s)$ (condition 1 of *Table* 1).

The local velocity distribution is found anisotropic along y direction. As shown in Fig. 3, the local velocity distribution of v_y is asymmetric for each bin in y direction, while the distribution of v_x in each bin remains symmetric. The local velocity distribution of v_y in the bins near the two boundaries $\widetilde{y} = 0$ or 1 ($\widetilde{y} = y/L$) shows remarkably asymmetric. While moving away from the driving wall, the asymmetry of the profile of the local velocity distribution v_y becomes less profound. In the box center, the profile becomes symmetric, while the boundary effect maybe balanced out.

For a quantitative analysis of the asymmetry, momenta technique of statistic distribution can be used and skewness is calculated for each local profile. The result is shown in Fig. 4. The

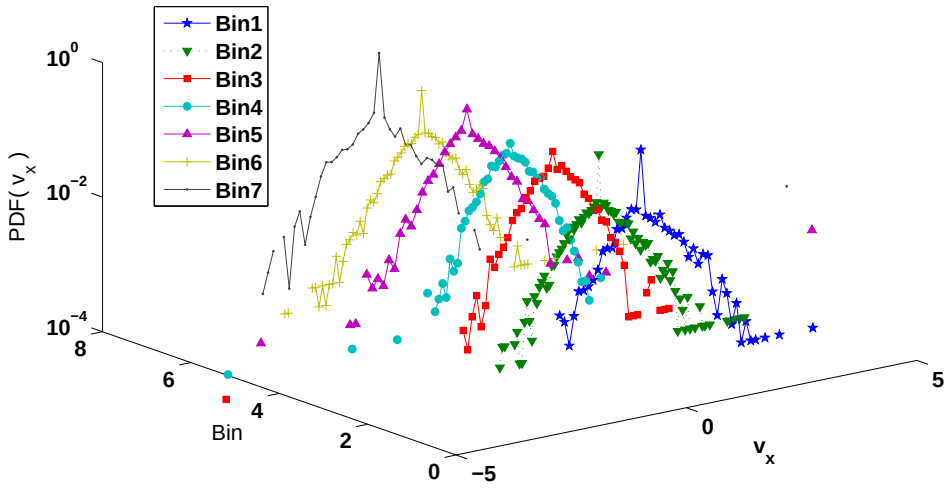

(a)

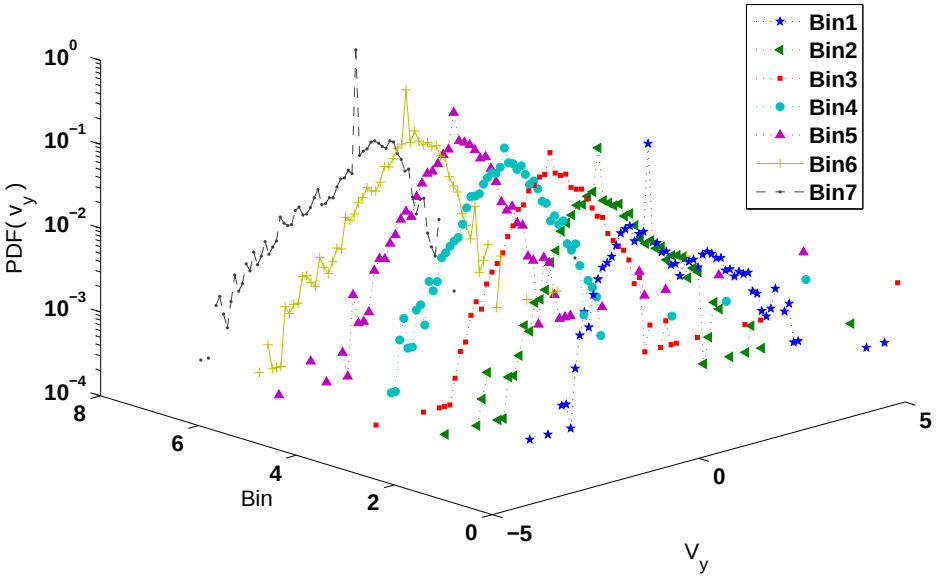

(b)

Figure 3: Local distribution functions of (a) v_x and (b) v_y in data set no. 1 of *Table 1*. There are 7 bins along the vibration direction y axis. The velocities are scaled by $V_\omega(0.07m/s)$.

skewness of n sample points x_i is defined as:

$$skewness = \frac{\frac{1}{n}\sum_n^{i=1}(x_i - \bar{x})^3}{(\frac{1}{n}\sum_n^{i=1}(x_i - \bar{x})^2)^{3/2}} \tag{1}$$

where $\bar{x}$ is the mean of all the n sample points x_i. Fig. 4 compares the skewness of profiles for v_x and v_y in different bins along y axis. The skewness is changing linearly from positive to negative and is about zero at the center of the box for v_y profiles, while skew seems flat for v_x

profiles.

In the steady state, conservation of momentum requires [20]:

$$\int_{-\infty}^{+\infty} vf(v)dv = 0, \tag{2}$$

therefore,

$$\int_{0}^{+\infty} vf(v)dv = -\int_{-\infty}^{0} vf(v)dv. \tag{3}$$

In turn, near the boundary $y = 0$, the number of particles moving towards the wall and leaving the wall shall be conserved [20, 21], that is, the particle number leaving the vibrating wall shall be equal to the particle number moving towards the vibrating wall in a sawtooth excitation:

$$f_y^-(v_y)v_y = f_y^+(2V_\omega - v_y)(v_y - 2V_\omega) \tag{4}$$

Here, f_y^+ (f_y^-) is the velocity distribution function for the $v_y > 0$ ($v_y < 0$). The number density n near the boundaries can therefore be obtained from particle-number conservation mentioned above [21]:

$$n_y = n_y^+ + n_y^- = \int_0^\infty f(v_y)dv_y + \int_{-\infty}^0 f(v_y)dv_y \tag{5}$$

At the boundary $y = 0$:

$$n_y = 2n_y^- + 2V_\omega \int dv_y \frac{f_y^-}{v_y - 2V_\omega} \tag{6}$$

It implies at the boundary $y = 0$, n_y^+ is smaller than n_y^-. The discrepancies between n^+ and n^- can be confirmed in our experimental results shown below(Fig. 7 (a) and (b)).

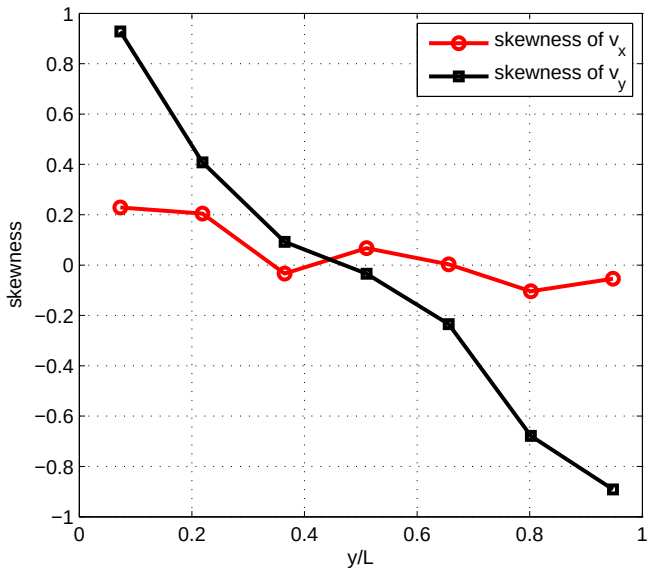

Figure 4: The skewness of v_x and v_y distribution profiles along y/L.

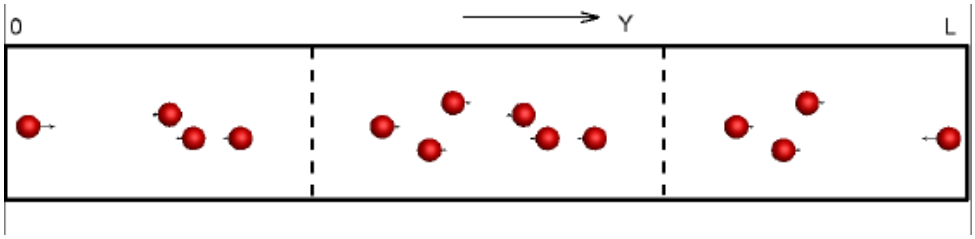

Figure 5: Sketch of the breakdown of the mean free path. On the right and left sides of the cell, the v_y distribution is asymmetric, contrary to what occurs in the cell center. As there is no net flow, it means the number density n^+ and n^- are different. This imposes to define two mean free paths through $n^- dl_c^+ = n^+ dl_c^- = 1$.

3.3. The breakdown of the mean free path

Mean free path is a basic concept in the kinetic theory. It is defined as the average distance the particle travels between two successive collisions. More importantly, the mean free path is often used to be a parameter to judge the suitable scope of the kinetic theories and hydrodynamics for granular medium [26]. The concept of mean free path is based on the assumption of particles being in random distribution, i.e., Maxwell-Bolzmann distribution is valid. However, in our system, the velocity distribution is no longer the Maxwell-Bolzmann distribution. Moreover, the local velocity distribution is asymmetric and anisotropic. This indicates the breakdown of kinetic models based on the concept of the mean free path.

At the cell wall, for instance, while the asymmetry of velocity v_y is the largest, one has to define two mean free paths, l_c^+ and l_c^-, for the two "kinds" of particles with v^+ and v^-, as demonstrated in Fig. 5. In Fig. 5 on the right and left sides of the cell, the v_y distribution is asymmetric, contrarily to what occurs in the cell center. As the average flow is zero, it means the density number n^+ and n^- are different. So this imposes the need to define two mean free paths that $n^- dl_c^+ = n^+ dl_c^- = 1$ (d is the particle diameter).

4. Hydrodynamic description

Starting from the measured positions (x, y) of particles and the velocities in four components $v_x^+(v_x > 0)$, v_x^- $(v_x < 0)$, v_y^+ $(v_y > 0)$, and v_y^- $(v_y < 0)$, the hydrodynamic parameters p_x^+ (p_y^+), p_x^- (p_y^-), n_x^+ (n_y^+), n_x^- (n_y^-), T_x^+ (T_y^+), T_x^- (T_y^-) can be derived from velocity components using the four sets of the experimental data shown in *Table 1.* In general hydrodynamics, the pressure p is considered as a symmetric tensor; we show here that p^+ is different from p^-, that means p is not single valued, so p is not a valid concept anymore.

4.1. The spatial profile of pressure

We will use the following notation $p_x^+(y) = \sum (v_x^+)^2(y)$ to present the pressure due to the x component with sum of v_x component with sum of v_x^2 for $v_x > 0$ of each bin along y direction. The mass of the particles are assumed to be unitary, $m = 1$. The pressure is scaled by $p_0 = (N/7)k_B T_{drive}$, where $N = 47$, $T_{drive} = V_\omega^2$, and V_ω is the peak value of the vibrating velocity, shown in *Table 1.*

For the p_x components it is observed that $p_x^+(y) \approx p_x^-(y) \approx$ *constant* (data are not shown here). However, the y components shown in Fig. 6 is rather unexpected. Firstly, the components of pressure p_y are no long constant in steady state [19, 20]. This result is also found in some simulation [27]. Secondly, in the vibrating direction, $p_y^+(y)$, $p_y^-(y)$ are asymmetric with respect to the center of the cell, and $p_y^+(y)$ and $p_y^-(y)$ are mirror symmetric to each other. Therefore, the pressure must be (i) anisotropic $(p_x \neq p_y)$, and even more (ii)$p_y^+ \neq p_y^-$. Point (ii) is linked

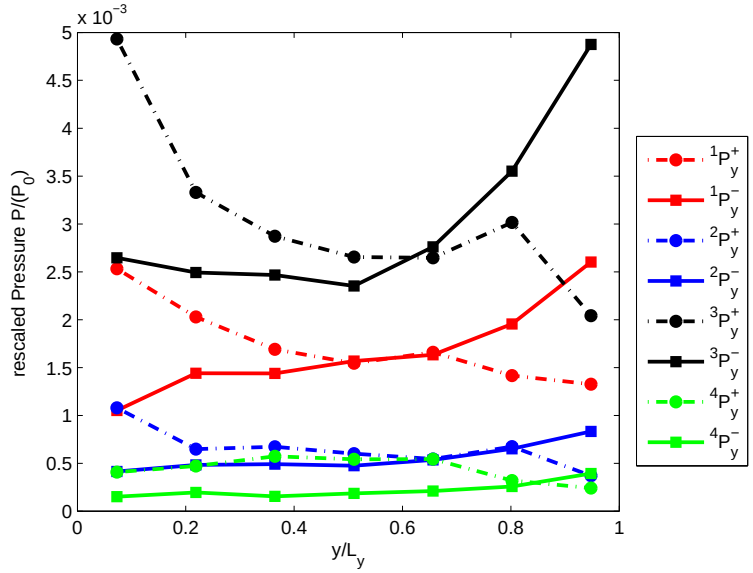

Figure 6: The scaled pressure $p_y^{\mp}(y)$ are plotted in the four sets of vibration parameters shown in *Table* 1.

to the asymmetric velocity distribution and to equation 2. This imposes $p_y^+ \neq p_y^-$ in such a system. Moreover, it is found that p_y components are always larger than p_x components.

From another view point, the pressure can be viewed as the kinetic energy in unit volume. So Fig. 6 can be seen as the energy profiles of the system. Obviously, $p_x^+(y)$ and $p_x^-(y)$ gain energy from the components in y direction to balance the energy dissipation in the x direction. In y components, $p_y^+(y)$ and $p_y^-(y)$ get energy from the two boundaries to balance the energy dissipation in the y direction and the energy transformed to the x direction. The difference $p_y^+(0) - p_y^+(L)$ as shown in Fig. 6 due to the energy dissipation along the y direction plus the energy being transformed to x direction.

4.2. Density inhomogeneity

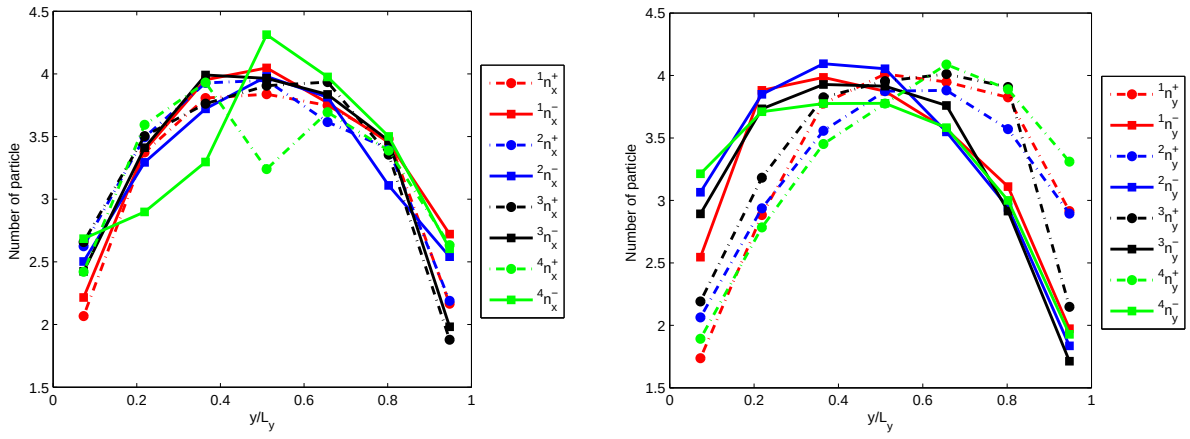

(a) (b)

Figure 7: The number density of particles (a) with velocity $v_x^{\pm}$ (b) with velocity $v_y^{\pm}$ are plotted in the four sets of vibration parameters shown in *Table* 1.

The number density with four components $n_x^+(y)$, $n_x^-(y)$, $n_y^+(y)$, $n_y^-(y)$ are shown in Fig. 7. The notation of $n_x^+(y)$ means the spatial profile of the number density of particles with velocity $v_x > 0$ along the y direction. We observe that $n_x^+(y)$ and $n_x^-(y)$ overlap and peak at the cell center as in Fig. 7(a). The curves in Fig. 7 (b) conform that the difference between $n_y^+(y)$ and $n_y^-(y)$ near the boundaries predicted in equations (3) and (4). Moreover, n_y^+ and n_y^- do not overlap. The components $n_y^+(y)$ and $n_y^-(y)$ are mirror symmetric to each other as shown in Fig. 7(b). It is apparent that $n_y^+(y) = n_y^-(y)$ is not in generally valid as assumed by the theoretician when calculating the transport parameters in granular system [1, 26].

4.3. Granular temperature

The temperature anisotropy due to the non-isotropic driving in vibro-fluid granular systems has been discussed in recent years [22, 27–30]. Here, $T_x^+(y)$ (T_x^-(y)) represents the average of v_x^2 for $v_x > 0$ ($v_x < 0$) groups of each bin along y direction. We observe that $T_x^+(y) \approx T_x^-(y)$, and $T_x^+(y)(T_x^-(y))$ are axisymmetric with central axis of the cell (it is not shown in this paper). However, $T_y^+(y)$ ($T_y^-(y)$) is asymmetric along y axis. The values of y component $T_y^+(y)$ ($T_y^-(y)$) is seen greater than that of the x components $T_x^+(y)$ ($T_x^-(y)$). $T_y^+(y)$ ($T_y^-(y)$) is greater near the boundary at $y = 0$ ($y = L$) as shown in Fig. 8. In Ref [30], an explanation is provided about the temperature anisotropy. However, in the paper, a Gaussian distribution was assumed. The non-Gaussian and asymmetric velocity distribution observed in our system imply the Gaussian distribution misleading. Our velocity distribution already verify a non-Gaussian existed. It means Gaussian distribution approximation is misleading in [30]. Temperature anisotropy is apparent, and the two components T_y^+ and T_y^- are mirror symmetric to each other.

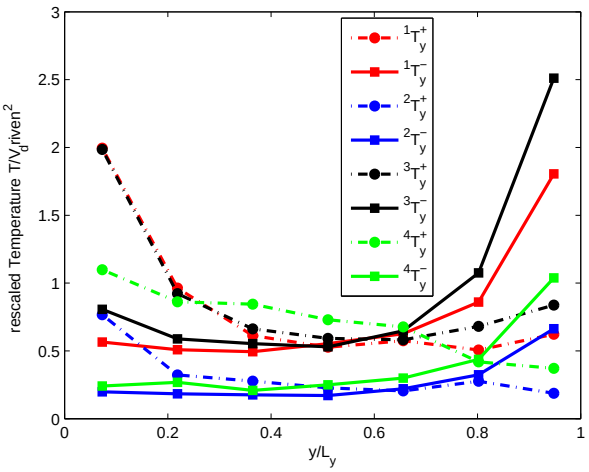

Figure 8: The scaled temperature $T_y^{\mp}(y)$ are plotted in the four sets of vibration parameters shown in *Table* 1.

5. Summary

The objective of this work is to provide an experimental study of the boundary effect in vibro-fluidized granular gas system. We have studied the velocity distribution in the vibration direction locally and globally. The velocity distribution is found anisotropic, and both its x and y components are non-Gaussian. We measure the local velocity distribution along the vibration direction and find that the v_x distributions are still symmetric, while the v_y distributions become asymmetric. The skewness of the profiles is found linear along y with skew = 0 at the cell center. This implies a long range boundary effect. The particles number density is found not a constant but peaked at the center. The hydrodynamics-parameter profile, $p_x^+(y)$ and $p_x^-(y)$, $T_x^+(y)$ and $T_x^-(y)$, $n_x^+(y)$ and $n_x^-(y)$ are overlapped, but the $p_y^+(y)$ and $p_y^-(y)$, $n_y^+(y)$ and $n_y^-(y)$, $T_y^+(y)$

and $T_y^-(y)$ are found mirror symmetric to each other. The asymmetry in the y component profiles can be understood as the dissipation of the energy input through collision with the boundary walls and energy transformed to x component through particles collisions. This long range boundary effect complicates the statistical properties of the confined fluidized granular gas system, and suggests further hydrodynamical studies are essential.

Acknowledgements
The authors want to thanks Novespace for helpful technical assistance and CNES for the fund of three years. This research was supported by CNES, ESA, ECP, CNRS, CAS, and CNSA for partial funding.

References

[1] Grossman, E. L. and Zhou, Tong and Ben-Naim, E. 1997 *Phys. Rev. E* **55** 4200
[2] Sergei E. Esipov, Thorsten Poeschel 1997 *J. Stat. Phys* **86** 1385
[3] Olafsen, J. S. and Urbach, J. S. 1999 *Phys. Rev. E* **60** 2468
[4] Olafsen, J. S. and Urbach, J. S. 1998 *Phys. Rev. Lett.* **81** 4369
[5] Rouyer, Florence and Menon, Narayanan F. 2000*Phys. Rev. Lett.* **85** 3676
[6] Kudrolli, A. and Wolpert, M. and Gollub, J. P., 1997 *Phys. Rev. Lett.* **78** 1383–1386 *Granular Matter*, **2**, 189
[7] Losert, W. Cooper, D. G. W. Delour, A. Kudrolli, J. P. Gollub 1999 *Chaos* **9** 682
[8] M. Hou, R. Liu, G. Zhai, Z. Sun, K. Lu 2008 *Microgravity Sci Technol* **20** 73-80
[9] Noije, T.P.C. and Ernst, M.H 1998 *Granular Matter* **1** 57
[10] Brey, J. Javier and Ruiz-Montero, M. J. and Cubero, D. 1996 *Phys. Rev. E* **54** 3664-3671
[11] Huthmann, M.,Orza, J. A., and Brito, R. 2000
[12] P. Evesque 2005 *poudres & grains* **15**,1
[13] P. Evesque 2007 *poudres & grains* **16**,3
[14] P. Evesque 2001 *Poudres & Grains* **12** 17-73, 60-82
[15] P. Evesque 2002 *Poudres & Grains* **13** 40-73
[16] P. Evesque 2004 *Poudres & Grains* **14** 8-53
[17] P. Evesque 2005 *Poudres & Grains* **15** 1-16,18-34
[18] P. Evesque 2007 *Poudres & Grains* **16** 38-62
[19] R. Liu, M. Hou, P. Evesque 2009 *poudres & grains* **17**,1
[20] P. Evesque 2010 *poudres & grains* **18**,1
[21] Brey, J. Javier and Ruiz-Montero, M. J. and Moreno 2000 *Phys. Rev. E* **62** 5339
[22] Herbst, Olaf and Muller, Peter and Otto, Matthias and Zippelius, Annette, E. 2004 *Phys. Rev. E* **70** 051313
[23] Du, Yunson and Li, Hao and Kadanoff, Leo P. 1995 *Phys. Rev. Lett.* **74** 1268
[24] Goldhirsch, I. and Zanetti, G. 1993 *Phys. Rev. Lett.* **70** 1619
[25] M. Leconte, Y. Garrabos, F. Palencia, C. Lecoutre, P. Evesque, D. Beysens 2006 *Appl. Phys. Lett.* **89** 243518
[26] Nikolai V. Brilliantov Thorsten Pöschel 2004 *Kinetic Theory of Granular Gases* (NewYork: Oxford University Press).
[27] J. Javier Brey, and D. Cubero 1998 *Phys. Rev. E* **57** 2019
[28] Barrat, Alain and Trizac, Emmanuel 2002*Phys. Rev. E* **66** 051303
[29] McNamara, Sean and Luding, Stefan 1998*Phys. Rev. E* **58** 813
[30] D. van der Meer , P. Reimann 2006 *Europhys. Lett.* **74(3)** 384-390